EUROPEAN LABORATORY FOR PARTICLE PHYSICS

LHCb 2000–31
CALO
24 June 2000

Experimental Performance of SPD/PS Detector Prototypes

S. Filippov, Yu. Gavrilov, E. Guschin[a)], S. Laptev, V. Postoev

Institute for Nuclear Research
Russian Academy of Sciences
60th October Anniversary Prospekt 7A
RU–117312 Moscow

LHCb Collaboration

Abstract

We describe current status of the development of Scintillator Pad Detector and PreShower detector prototypes for the LHCb experiment at CERN. SPD/PS consists of two identical layers of scintillator pads with a lead converter in between. The pads are read–out by single WLS fibres coiled in a groove in the scintillator body. Experimental results obtained with several prototypes during 1999–2000 years are described.

[a)] Corresponding author, E–mail: Evgueni.Gouchtchine@cern.ch

1 Introduction

Scintillator Pad Detector (**SPD**) and PreShower (**PS**) detector are parts of calorimetry system of the LHCb [1] experiment. Main purpose of the PS is to complete electron/hadron separation obtained with ECAL at the level-0 trigger. The SPD selects charged particles from neutrals at the entrance of calorimeters, providing necessary information for gamma trigger. Both detectors also provide valuable information for the off-line analysis stage. Being different by read-out electronics and trigger parts, from the point of view of the detector technique, both SPD and PS consist of essentially identical systems of scintillator pads read-out by WLS fibres and equipped with multi-anode PMTs. Therefore, by the construction, they are considered as one detector unity. Performance and design of the prototypes being developed and tested by INR (Moscow) group during last two years are described in this note. The content of the note is outlined as follows:

- **Sec. 2**. Requirements and layout of the detector.
- **Sec. 3**. Optimisation of detector cell design and choice of scintillator/fibre technique.
- **Sec. 4**. Experimental results with SPD/PS prototypes.
- **Sec. 5**. Some results of experimental study of multi-anode photomultiplier tube (MAPMT) read-out.
- **Sec. 6**. Durability and radiation hardness.
- **Sec. 7.** Summary of the results on performance and plans for future tests and prototypes.

2 Preshower detector layout and requirements

The detector layout is described in [2]. Basic dimensions of the cells are $\sim 4 \times 4$, 6×6 and 12×12 cm^2. The cells are assembled in module units of 49×49 cm^2 and connected by clear fibres of 1-3 meters long to PMTs. The amount of collected light from MIP should provide the necessary performance:

- π/e rejection with 95% efficiency for electrons, with the pions retaining fraction below 10%.
- More than 95% of MIP registration efficiency at the threshold of 0.5 MIP.
- Short time response with at least 80% of charge integrated within 25 $nsec$.
- $10\%/\sqrt{E}$ stochastic term of ECAL energy resolution with PS.
- To fulfil the above requirements light yield is to be more than $15-20$ $ph.\ el.$/MIP.

3 Optimisation of light collection

The optimal design depends on cell size, quality of scintillator, machining etc. In order to optimise light collection and get fast time response a set of preshower prototypes was produced and tested in X7 (SPS) test beam at CERN. Total number of measured prototypes was close to 100, taking into account combinations of all variations of design, types of fibre/scintillator, wrapping and coupling. Nevertheless, it was not enough to pretend on complete systematic study of light collection as function of all possible parameters, like number of fibre coils, pad dimension, design, etc. Therefore the goal was to concentrate the work on studies of the options close to the "working point" such as fixed scintillator dimensions except two variants of thickness, two types of groove design, conventional types of fibre/scintillator and optical contact in order to prove the presumably optimal choice.

3.1 Choice of fibre layout. Design of prototypes.

Studies of light collection in scintillator tile with WLS fibre read-out have been done by many groups [3]. Some of them, like CDF, CMS, OPAL endcaps, make optimisation of WLS fibre layout for tiles of significantly larger dimensions then in LHCb SPD/PS. Other experiments with small like in LHCb scintillator cells (WA93, WA98) use simple variant of design with straight fibres, that has not optimal light collection efficiency per read-out fibre unit. Design optimisation through Monte-Carlo simulation is not precise unless all the parameters of optical model are determined. Therefore the experimental studies of prototypes with various fibre layouts were done in X7 LHCb test beam in June–July of 1999.

The idea was to optimise the following parameters of the design:

a. Number of fibre turns (1–7 turns) that is important for time duration of the signal. Typical speed of the light propagation along the fibre is about 5 $nsec/m$.

b. Fibre layout, shown in Fig. 1 from the top to the bottom:
1) fibre coiled in scintillator depth inside the "DEEP" groove
2) fibre running through scintillator in "HELIX" groove (see also Fig. 2).

c. Thickness of scintillator. Comparison was done for 10 mm vs. 15 mm.

d. Cell size: 40×40 mm^2 and 120×120 mm^2.

e. Type of scintillator, comparing PolyVinylToluene (**PVT**) BC-408 vs conventional cast polystyrene (**PS**) scintillator produced in Russia.

f. Type of WLS fibre: Y11(250) MC S-type vs. BCF91A MC.

g. Wrapping with Tyvek vs. DMA attacked scintillator surface. Aluminization of the lateral sides was also tested.

h. Optical contact between the fibre and the scintillator: BC-600 glue vs. BC-630 optical grease, or air contact.

Basic idea of the preshower prototypes design is shown in Fig. 1. We compare two best variants: "DEEP" groove, when WLS fibre makes several (2-4) coils in the rectangular groove machined on large side of scintillator pad, and more complex "HELIX" one (Fig. 2), when scintillator consists of two parts: outer part with a hole plugged by inner cylindrical part. The fibre runs by groove milled on inner surface of outer part. For better contact between fibre and scintillator optical grease (BC-630) or glue (BC-600) was used. We compared these two design approaches for various cell dimensions, thickness, number of fibre coils and scintillator types.

3.2 Experimental set-up and method.

1. We installed scintillator cells in the X7 beam one by one with the same PMT (FEU-85, Russia). It's quantum efficiency at 500 nm was estimated as $12-15\%$. WLS fibres ends of $\sim$ 10 cm long were always coupled to the PMT centre (Fig. 1). No clear fibres were used for this test. We found that optical grease BC-630 can improve fibre-to-PMT optical contact by $\sim 10\%$. The reproducibility of the fibre-to-PMT contact was $\sim 5\%$ (r.m.s.). Therefore all significant results were averaged over a few sets of repeated measurements.

2. We used 11-bits LeCroy ADC 2249A for charge measurement. The width of the ADC gate was $\sim$ 150 $nsec$, surely enough to integrate total charge. Length of signal cables was about 30 meters.

3. Despite of the same HV value used for all measurements (920V), we found that it was necessary to control the gain of the PMT. For gain monitoring signal from alfa-particle source ^{238}Pu evaporated on $YAlO_3$ crystal was used. The crystal was glued close to the edge of the PMT photo-cathode window.

4. Absolute scale of the light signal in terms of photo-electrons was obtained with LED flashing WLS fibre $\sim$ 15 cm from PMT. Relative width of LED spectrum was taken as statistical fluctuations of the number of photo-electrons. We did not correct it for gain fluctuations (excess noise factor) of PMT, which could be equal to $1.5-2\%$ for this type of photomultiplier. As MIP signal the most probable value of the signal was taken, as less dependent on the type and momentum of beam particles.

5. We used 50 GeV/c electrons and 120 GeV/c muon beams. The beam spot was $\sim 4\times 4$ cm^2, with rather uniform statistical population. For the light collection measurements selected beam position was $\sim 2\times 2$ cm^2 at the scintillator centre. For uniformity studies of small pads, beam spot was spread over the surface of the scintillator cell. For 120 mm detectors, they were exposed in the beam at the centre and at the corner, as shown in Fig. 4.

3.3 Measurements.

1. First measurements of the light response to MIPs were done for prototypes made of cast polystyrene from Russia. The summary of the results is shown in Table 1. Prototypes were equipped with 1 *mm* diameter BCF91A (MC) fibre. We compare two types of groove ("HELIX" and "DEEP") for various number of fibre turns. No grease or glue was used for optical coupling between the scintillator and the fibre. All prototypes were wrapped with two layers of TYVEK (0.15 *mm* thick). As it can be seen from Table 1, the light output is not significantly changed with number of fibre turns. One half of fibre turn appears due to the fact that both ends of the fibre must come to the same side. It was also measured that design of groove does not affect sizably the light output.

Table 1: Light yield of polystyrene scintillator with BICRON fibres without grease/glue in the groove.

Number of fibre turns	Type of groove	Dimension (mm)	Scintillator type	Fibre type	Sci/fibre coupling	Number of ph.el./MIP	Cover
0.5	deep	$120 \times 120 \times 10$	PS	BCF91A	air	19	Tyvek
1.5	deep	$120 \times 120 \times 10$	PS	BCF91A	air	23	Tyvek
2.5	deep	$120 \times 120 \times 10$	PS	BCF91A	air	32	Tyvek
2.5	helix	$120 \times 120 \times 10$	PS	BCF91A	air	30	Tyvek
3.5	helix	$120 \times 120 \times 10$	PS	BCF91A	air	39	Tyvek
0.5	deep	$120 \times 120 \times 15$	PS	BCF91A	air	31	Tyvek
1.5	deep	$120 \times 120 \times 15$	PS	BCF91A	air	34	Tyvek
2.5	helix	$120 \times 120 \times 15$	PS	BCF91A	air	45	Tyvek
3.5	helix	$120 \times 120 \times 15$	PS	BCF91A	air	58	Tyvek
1.5	deep	$40 \times 40 \times 10$	PS	BCF91A	air	51	Tyvek
2.5	deep	$40 \times 40 \times 10$	PS	BCF91A	air	58	Tyvek
2.5	helix	$40 \times 40 \times 10$	PS	BCF91A	air	57	Tyvek
3.5	helix	$40 \times 40 \times 10$	PS	BCF91A	air	59	Tyvek
6.5	helix	$40 \times 40 \times 10$	PS	BCF91A	air	56	Tyvek
1.5	deep	$40 \times 40 \times 15$	PS	BCF91A	air	74	Tyvek
2.5	helix	$40 \times 40 \times 15$	PS	BCF91A	air	83	Tyvek
3.5	helix	$40 \times 40 \times 15$	PS	BCF91A	air	85	Tyvek

2. We studied the effect of reflectivity of scintillator surface on light collection efficiency. The results are shown in Table 2. From comparison with data from Table 1 it was concluded that light collection in the case of chemically treated

scintillator surface (DMA) does not differ from TYVEK wrapping in case of $40 \times 40\ mm^2$ cell size. But in case of large cells light collection is better with TYVEK by $\sim 30\%$. In case of long scintillator plate it is qualitatively apparent that the transportation of light with diffusive reflection is to be less than with total internal reflection from polished surfaces. The advantage of DMA/aluminization usage is in reducing the gap between cells for detector layout. As for aluminization of lateral sides, it was measured that for a given quality of the evaporation of Al the light yield is by $20 - 50\%$ less than for TYVEK coating.

Table 2: Same as in Table 1 but scintillator was treated with DMA or small sides aluminized. Numbers in brackets are shown for comparison and were obtained with TYVEK coating.

Number of fibre turns	Type of groove	Dimension (mm)	Scintillator type	Fibre type	Sci/fibre coupling	Number of ph.el./MIP	Cover
3.5	deep	$120 \times 120 \times 10$	PS	BCF91A	air	29	DMA
1.5	deep	$40 \times 40 \times 10$	PS	BCF91A	air	47(51)	DMA
2.5	helix	$40 \times 40 \times 10$	PS	BCF91A	air	42(57)	DMA
3.5	helix	$40 \times 40 \times 10$	PS	BCF91A	air	58(58)	DMA
0.5	deep	$40 \times 40 \times 10$	PS	BCF91A	air	15	Alum
1.5	deep	$40 \times 40 \times 10$	PS	BCF91A	air	23(51)	Alum
2.5	helix	$40 \times 40 \times 10$	PS	BCF91A	air	28(57)	Alum
3.5	helix	$40 \times 40 \times 10$	PS	BCF91A	air	42(59)	Alum
0.5	deep	$40 \times 40 \times 15$	PS	BCF91A	air	18	Alum
1.5	deep	$40 \times 40 \times 15$	PS	BCF91A	air	31(74)	Alum
2.5	helix	$40 \times 40 \times 15$	PS	BCF91A	air	50(83)	Alum
3.5	helix	$40 \times 40 \times 15$	PS	BCF91A	air	45(85)	Alum

3. Effect of grease/glue optical coupling between Y11(250) MC fibre and scintillator was also studied. The data shown in Table 3 should be compared with those from Table 1. The BC-600 glue and BC-630 grease improve light collection by $\sim 30\%$ and give comparable results.

4. Comparison of PVT and PS scintillators and Y11 vs BCF91A multi-clad fibres were done. The data are presented in Table 4. As it was expected, the measurements confirmed that the light yield of BC-408 scintillator is better by factor of $1.5 - 1.6$ compared to polystyrene. But from cost and machining point of view polystyrene based scintillator has significant advantage. Therefore we

Table 3: Light yield of the polystyrene scintillator with Y11(250)MC fibres and BC-630 grease in a groove.

Number of fibre turns	Type of groove	Dimension (mm)	Scintillator type	Fibre type	Sci/fibre coupling	Number of ph.el./MIP	Cover
2.5	deep	$120 \times 120 \times 10$	PS	Y11	grease	42	Tyvek
2.5	helix	$120 \times 120 \times 10$	PS	Y11	grease	41	Tyvek
3.5	helix	$120 \times 120 \times 10$	PS	Y11	grease	48	Tyvek
2.5	deep	$40 \times 40 \times 10$	PS	Y11	grease	78	Tyvek
2.5	helix	$40 \times 40 \times 10$	PS	Y11	grease	82	Tyvek
3.5	helix	$40 \times 40 \times 10$	PS	Y11	grease	80	Tyvek
2.5	helix	$40 \times 40 \times 15$	PS	Y11	grease	110	Tyvek

keep PS scintillator as the base-line solution, compensating the lower light yield by increasing the thickness.

3.4 Summary of light collection results

As main results obtained with prototypes described above, it was found that:

1. For the same number of fibre coils the ratio of light yield of 12 $cm \times 12$ cm cell to that of 4 $cm \times 4$ cm cell is $\sim 2:3$.
2. Light yield is proportional to the thickness of the scintillator: 10 mm to 15 mm ratio is $\sim 2/3$.
3. Light collection with "DEEP" groove design gives the same result as "HELIX" one.
4. Optical grease BC-630 and optical glue BC-600 give identical results and improve the light yield by $\sim 30\%$.
5. PVT scintillator BC-408 produces ~ 1.6 times more light than conventional polystyrene scintillator manufactured in Russia.
6. Aluminization of small sides of the scintillator pad deteriorates the light collection.
7. Surface of the scintillator treated with DMA gives the same result as wrapping with TYVEK in case of small cells, but for 12 cm cells TYVEK becomes better.
8. Number of fibre turns equal to 3–4 gives the maximum light yield.

Table 4: Comparison the BC408 scintillator with polystyrene one.

Number of fibre turns	Type of groove	Dimension (mm)	Scintillator type	Fibre type	Sci/fibre coupling	Number of ph.el./MIP	Cover
2.5	deep	$120 \times 120 \times 10$	BC408	BCF91A	grease	71	Tyvek
3.5	deep	$120 \times 120 \times 10$	BC408	BCF91A	grease	69	Tyvek
2.5	deep	$40 \times 40 \times 10$	BC408	BCF91A	grease	90	Tyvek
3.5	deep	$40 \times 40 \times 10$	BC408	BCF91A	grease	91	Tyvek
2.5	deep	$40 \times 40 \times 10$	PS	Y11	grease	65	Tyvek
2.5	helix	$40 \times 40 \times 10$	PS	BCF91A	glue	63	Tyvek
3.5	deep	$40 \times 40 \times 10$	BC408	BCF91A	glue	90	Tyvek
3.5	helix	$40 \times 40 \times 10$	BC408	BCF91A	glue	90	Tyvek
1.5	deep	$40 \times 40 \times 15$	PS	Y11	glue	85	Tyvek
2.5	helix	$40 \times 40 \times 15$	PS	Y11	grease	110	Tyvek
3.5	helix	$40 \times 40 \times 15$	PS	BCF91A	glue	105	Tyvek
3.5	helix	$40 \times 40 \times 15$	PS	Y11	glue	102	Tyvek
3.5	helix	$40 \times 40 \times 15$	PS	Y11	grease	109	Tyvek

9. Typical value of light yield from the MIP for 4 fibre coils in $40 \times 40 \times 15$ mm^3 pad was measured ~ 100 ph.el./MIP as shown in Fig. 3.

10. Y11(250) double-clad S-type fibre from KURARAY [6] and BCF91A from BICRON [5] give about the same light yield, but Y11 S-type has better mechanical properties[7].

11. Grease contact of fibre with the PMT window gives by $\sim 10\%$ more light but the grease is hardly applicable in a long term experiment.

3.5 Lateral uniformity of response

3.5.1 Uniformity of 120×120 mm^2 cells

We measured the response of scintillator pads to 50 GeV/c electrons at two positions (Fig. 4). The size of the beam spot was about 4×4 cm^2. Comparison between signal at the centre and at the corner of a scintillator cell is shown in Fig. 5. Two large size prototypes with dimensions $120 \times 120 \times 10$ mm^3 wrapped with TYVEK paper with 2 and 3 turns of fibre in "DEEP" groove were measured. The response at the centre was found by $\sim 6 - 7\%$ smaller than at the corner of the detector.

3.5.2 Uniformity of 40×40 mm^2 cells

Uniformity of the 40×40 mm^2 cells was measured with wide 120 GeV/c muon beam spread over surface of the detector. Taking into account more compact design of a small pad, one can expect the global uniformity for it should be better than for a large pad. The only effect to be investigated is the cell response near the fibre, i. e. at a few percent of the detector surface. There are two factors playing against each other: in the groove region the scintillator thickness is smaller and therefore the energy losses are less. But the light collection is more efficient, because of the fibre is closer to the particle track. The last effect is less important for smaller cell dimensions and larger thicknesses.

In Fig. 6 one can see the response of 10 mm thick cell made of BC408 scintillator with 4 coils of fibre in "DEEP" groove as a function of the distance from the centre of the cell. Beam particle coordinates were measured with accuracy of 0.5 mm in Y direction and 3 mm in X. In the region of groove at $R = 17.5$ mm the response drops by factor of ~ 2 due to reduced thickness of the scintillator in the groove (≈ 5 mm).

This effect becomes smaller for cells with 15 mm thickness, as it is shown in Fig. 7. Less number of coils and less deep groove can improve the local uniformity of response around the fibre coils. Case of two fibre coils is shown in Fig. 8.

As the conclusion on uniformity measurements, we can underline the following:

1. Response of the large cell has global variation of $2 - 3\%$ (r.m.s.). Signal at the centre of 120×120 mm^2 cell is smaller by 7% compared to the one in the corner.

2. Global uniformity of the response for the small cell is better then for the large one.

3. The scintillator thickness 15 mm is preferable due to the less drop of the signal in the groove area.

4. The design with "DEEP" groove provides better uniformity and hermeticity then with "HELIX" one, because there is no cracks and no particles leaking through the cell without giving a signal. Fibre coils are more compactly packed inside the "DEEP" groove and therefore the scintillator thickness is more uniform.

5. Design with $2 - 4$ fibre coils allows to obtain a good uniformity of response ($2 - 3\%$ deviation) and $\sim 100\%$ efficiency for charge particles registration with ~ 0.5 MIP threshold.

3.6 Choice of basic design of the pad

3.6.1 Type of scintillator

The PVT scintillator BC-408 (BICRON) gives $\sim$ 1.6 times more light than conventional polystyrene scintillator produced in Russia. But polystyrene scintillator is

simpler for machining and cheaper. Our experience with machining of BC408 shows that even careful milling of the groove can produce defects ("freeze") on the polished surface near it. Therefore, giving the same amount of light, 15 mm thick PS scintillator looks preferable then BC-408 with 10 mm thickness.

3.6.2 Scintillator thickness

Our measurements confirm that the light signal is proportional to the thickness. The final choice on the thickness should be done taking into account that:

1. Mechanical design allows to increase the thickness up to 15 mm. Inclined tracks at the region of the boundaries between two cells will fire both cells more often for larger thickness. Unless a study of this effect with Monte-Carlo gives constrains on the thickness, the light yield is the most important parameter and the 15 mm should be chosen.

2. Due to the same fact the sum of responses of thick cells will be more uniform for the same gap width between pads;

3.6.3 Type of fibre

The Y11 multi-clad S-type fibre is the only one commercially available now, which satisfies all the requirements: a) light yield; b) mechanical durability; c) radiation hardness; d) fast response. The cheaper BCF91A fibre has less mechanical stability against bending at small radius and is slower.

3.6.4 Number of fibre coils

The length of the fibre coupled to scintillator increases the signal duration by $\sim 5\ nsec/m$. Due to the short attenuation length in bended fibre ($\sim 50-100\ cm$), light collection is not proportional to fibre length and even comes down for large number of coils. We choose 3-4 fibre turns as close to the optimal value.

3.6.5 Type of groove design

We found no significant difference in the light collection between two options of the design: "DEEP" and "HELIX" groove. We choose the former one for the final design as more simple and cheap for machining, assembly and gluing. Moreover, as shown in Sec 3.5, the uniformity of MIP response in the groove region was found to be better with "DEEP" groove design.

4 Experimental results with matrix prototypes

4.1 Prototypes description

In order to study technological issues and to test the SPD/PS detector performance in combined test two matrix prototypes were built in the summer of 1999. The pictures in Fig. 9 and 10 show the view of assembled module prototype. It consists of 3×3 inner matrix of 4×4 cm^2 cells and 8 surrounding cells of 12×12 cm^2 size, packed in light-tight black box totally made from epoxy armed with carbon fibre. The thickness of the box walls was 250 μm, that is close to the final design requirements.

The prototypes differ from each other just by the thickness and type of the scintillator: 10 mm thick BC-408 scintillator (BICRON) and 15 mm thick polystyrene based cast scintillator (Russia). From the results of tests described above about the same light response was expected from both prototypes. Our plan was to compare the behaviour of the signal in the region of gap between adjacent cells with different incident angles for these two values of scintillator thickness. This point was not executed during the combined test due to the lack of time and bad precision of beam particles coordinate measurement. We intend to do this during beam tests 2000.

Scintillator pads were wrapped with 150 μm thick TYVEK paper. We used WLS Y11(250) multi-clad S-type fibre of 1 mm diameter coiled in "DEEP" groove with 3 turns. The fibre was glued into the scintillator by BC-600 optical glue (BICRON). Each end of WLS fibre of ~ 30 mm long was coupled to the 1 mm diameter clear fibre (KURARAY) by an individual optical connector. The length of clear fibres was 3 meters. The bundle of 34 fibres from each module box was packed into light-tight black pipe. The other ends of clear fibres were connected to 64-anode PMT (R-5900, HAMAMATSU [4]). All ends of clear fibres were gathered to the PMT window by means of optical coupler made of plastic with 64 pairs of drilled holes.

The pixel size of the PMT is 2×2 mm^2 and for better coupling the two corresponding holes were disposed by the pixel diagonal. Each fibre end was flatly cutted and polished. Then it was tightly inserted (without glue) into the individual hole and pressed to the cathode window. There was no grease coupling used between fibre and the PMT window. The two fibres from each scintillator cell were connected to the corresponding pixel of PMT. The coupler was visually positioned by use of PMT marks supplied by manufacturer. The precision of the coupler alignment with respect to the PMT pixels was ~ 0.2 mm. As soon as there were no means foreseen for the precise control of fibres position with respect to the PMT pixels, some part of the light cross-talk measured during the tests could be attribute to bad optical coupling. That is another subject to be studied in the future tests.

4.2 Beam test description and experimental program

Module prototypes of the SPD/PS detector were tested together with ECAL and HCAL prototypes in October 1999 at the X7 test beam line. The module with polystyrene scintillator used mainly as SPD was installed in front of 1 cm thick lead

converter. The module with BC-408 scintillator (PS) was installed right behind the lead converter and approximately 10 cm in front of 3×3 ECAL towers assembly. Both modules were aligned with ECAL and each other. All the prototypes were situated on the moving platform, that allowed to scan the horizontal and vertical position with better than 1 mm accuracy. The beam was changed to $5-100$ GeV electrons, pions and muons. Unfortunately the sufficient DAQ rate was available only with medium energies $10-50$ GeV. Therefore the π/e separation at interesting for LHCb energies below 10 GeV was not studied.

4.3 Experimental results

4.3.1 π/e rejection

As far as electrons start showering in the lead converter they produce significantly larger signals in PS scintillator then pions since they pass it without interaction (only $\sim 10\%$ of them interact in 1 cm of lead). The threshold applied to signals in PS provides separation of pions and electrons. In Fig. 11 one can see π/e rejection for 10, 20 and 50 GeV obtained with PS. To clear electron or pion trigger information was used from two Cherenkov counters of X7 beam line as well as from muon hodoscope positioned behind the HCAL. Geometrical acceptance was defined by SPD cell of 40×40 mm^2 just before the PS detector unit. Effect of pion rejection improvement when high signals in SPD are cutted is discussed in the next chapter. Preshower alone provides $\sim 92-93\%$ rejection of pions if cut set at 100-150 ADC counts (4-7 MIPs) with 95% electrons accepted (see Table 5).

Table 5: Rejection of pions in PS with 95% electrons accepted.

Particle	10 GeV	20 GeV	50 GeV
electrons	95%	95%	95%
pions	7.5%	7%	8%

If information from ECAL is added and particle momentum is known, more pions can be rejected. As an example, the rejection of pions with PS and ECAL information used is shown in Fig. 12. The cuts shown select 92% of electrons for PS signal $>$ 75 ADC counts (4 MIPs) and ECAL signal $>$ 610 ADC counts. Only 0.4% of pions shown as circles are taken as electrons. In the figure HCAL and SPD information is shown also. For 12 selected pions that pass the cuts in PS and ECAL as electrons, HCAL and SPD signals are shown in the insets. One can see that these pion events look also as electrons in HCAL and SPD. Fraction of pion events taken as electrons is defined by spread of electron signal in ECAL. Pion rejection with ECAL, assuming that particle momentum is precisely known, is shown in Table 6. Threshold for PS signal was set to 4 MIPs.

Table 6: Rejection of pions in PS with ECAL. PS threshold is 4 MIPs.

Particle	10 GeV	20 GeV	50 GeV
electrons	91%	92%	97%
pions	0.4%	0.4%	0.3%

4.3.2 Energy resolution with ECAL

Electromagnetic shower looses some part of its energy in the lead converter. This deteriorates energy resolution of ECAL. As soon as energy lost in lead is function of the number of particles in the shower part developed in lead, the PS signal from particles leaving lead can be used for energy loss corrections. From Monte-Carlo simulations it is expected that 1 *cm* of lead absorbs insignificant part of electromagnetic shower, particularly, in the beam energy range. Therefore the correction of ECAL response with PS signal is to be the minor one.

In Fig. 13 the data obtained with ECAL and PS with 20 GeV electrons are shown. The scatter plot shows the correlation between PS and ECAL signals that were used for the correction. On the upper-left plot events with small energy deposit in PS are selected. This plot characterises the ECAL energy resolution, if there is no lead in front. The upper-right plot shows all events, if there is no PS correction applied. Deterioration is small as we can expect from small thickness of lead absorber. Nevertheless it could be recovered by linear correction with PS signal (bottom-left).

4.3.3 MIP registration in SPD

Spectrum of signals from minimum ionising particles obtained in SPD matrix prototype is shown in Fig. 14. The registration efficiency obtained with a cut > 0.5 MIP for most probable value was larger than 98%. An experimental definition of the beam particle coordinates was not precise enough to measure the signal in the region of gaps between the cells. By the same reason the lateral uniformity of the response was not measured. We plan to repeat the measurements in better experimental conditions in the summer of 2000. Light collected from MIPs was estimated with a reference LED as $\sim$ 20 ph. el. for 120×120 mm^2 cell and $\sim$ 30 ph. el. for 40×40 mm^2 one. To compare the last value with that of 3.4(9), a few factors should be taken into account:

1. Light losses in optical connectors could be estimated as $\sim 0.87 \pm 0.03$ [10]. No systematic study of light losses was done for single-fiber connectors used in these tests because of multi-fiber type connectors are chosen for the future design [2].

2. Light leakage to neighbouring pixels for MAPMT of $\sim 0.8 \pm 0.05$. This number will be improved as it is discussed below 5.1.

3. Difference of photo-cathode sensitivity for FEU-85 and MAPMT R5900 at $500nm$ gives a factor of $\sim 0.75 \pm 0.03$.

4. Light attenuation of clear fiber of PSM [6] type for 3 meters at $500nm$ is a ~ 0.71.

5. Anode non-uniformity ~ 12 % of MAPMT gives additional uncertainty.

The final factor 0.37 ± 0.05 underestimates possible losses because the same optical coupler to PMT window was used in different tests and for this reason clear fibers were not glued.

4.3.4 Efficiency to electrons and pions. Cluster size in SPD.

One can see from Fig. 15 and 16 that the cluster size (number of fired cells) in SPD is significantly different for pions and electrons. It was found that it depends also on the fraction of energy deposited by particle in PS. Thus electron triggered in PS with threshold of 7 MIPs (94% at 20 GeV) gives signal in more than 5 cells of SPD in $\sim 5\%$ cases. As for 20 GeV pions passing the same PS threshold, they fire more than 5 cells in $\sim 35\%$ cases.

All these results were obtained with 3×3 inner matrix of $40 \times 40 mm^2$ cells with the beam in the central cell. The cross-talk between adjacent cells that was measured with LED signal as $\approx 20\%$ (sum of the signals from eight neighbouring cells), should be taken into account for interpretation of this result.

The registration efficiency (non-zero cluster) was found to be $\sim 98\%$.

4.3.5 Rejection of pions in SPD

In Fig. 17 signals from 50 GeV pions and electrons in PS and SPD prototypes are superimposed. Minimum ionising particles give signal about 18 ADC counts (most probable value). Spectrum of pion signal in SPD has longer high energy tail then signals from electrons. As interpretation, these events correspond to inherent inelastic processes in lead nuclei, when large number of low energy nucleons (neutrons, protons, alpha-particles) leave the nucleus. The part of them comes back to SPD giving the signal larger then 5-10 MIPs. This can be used for additional pion suppression in combination with PS cuts. In Fig. 18 the pion rejection and electron acceptance are shown for various thresholds for PS and cuts on SPD signal. It can be seen that at high energy even ~ 10 MIP SPD cut can improve pion rejection by factor of 2.

5 Multi-anode PMT read-out

The main features of multi-anode PMT R5900, like fast time response, good amplification, compact design and low price per channel, are explored in the current design of SPD/PS detector. Among the known drawbacks of MAPMT more distinguishable for

larger number of pixels are low linearity range, significant anode non-uniformity, that also limits dynamic range, and cross-talk between neighbour pixels. The SPD/PS module prototypes were read-out by H7546 (R5900-00-64 series) PMT. The outline of characteristics, provided by manufacturer, are:

- Base with 12 stages voltage distribution is designed by manufacturer for improved linearity: $3-2-2-1...1-2-5$.
- Anode uniformity over 64 pixels is better than 12% (r.m.s.) and highest/lowest ratio ~ 2 (see Fig. 19).

5.1 X-talk between the pixels of PMT.

Light leaving the fibre end with the angle to the fibre axis have a chance to propagate along the window and to give signal in the neighbour pixel. The value of such light leakage depends on the precision of the fibre-to-pixel coupling, the distance from the fibre end to the PMT window and of the thickness of the glass. Design of the coupler used in the described tests was based on the precise matrix of holes drilled in a plastic holder (fig. 9). Each pair of fibres from the same detector cell was coupled to the PMT pixel by its diagonal (fig. 20). The distance from the fibre edge to the pixel boundary is $\sim 0.2\ mm$. Each fibre is displaced to the corresponding pixel corner. Therefore the light leakage is larger for the pixels adjacent to this corner. In tables 7 and 8 the distribution of the light from one of the fibre in 3×3 pixels is shown. The measurement was done with the combined test setup. The super-bright blue LED was flushing through the diffusion coupler on the clear fibre connected to the central pixel. The distance between LED and PMT was 50 cm. The direct LED light leakage to other fibres was excluded. The data with various LED amplitudes are shown in Fig. 21. LED was illuminating the fibre coming to the PMT pixels 12 and 13. Signal from pixels is plotted vs the sum of signals from neighbour 8 pixels for each LED amplitude. About 20 and 25% of light from the illuminated fibre come to adjacent pixels. No light leakage to far pixels was observed.

Photo-statistical fluctuations of signal leakage has no visible correlation with the signal from the central pixel. This fact points out that the X-talk takes place before the multiplication process starts. It was also observed that average value of the X-talk does not depends on the signal amplitude.

Table 7: The light leakage, % from pixel N12 (at the centre) to the 8 neighbouring pixels.

1.0	1.3	1.6
10.5	75.2	0.9
2.5	5.5	1.5

Table 8: The same as in table 7 for pixel N13 at the centre.

0.5	2.5	0.6
6.9	80.9	1.2
1.4	5.4	0.6

The value of X-talk observed is rather large to be neglected. The part of its value results from misalignment of fibre-to-pixel positioning. As soon as there are two fibres read-out by one pixel in present design, some part of light leakage is unavoidable. The rest can be improved by better positioning of the coupler on the PMT window and by controlling the air gap between the fibre and the glass. We plan to study the optimal fibres-to-PMT coupling in May-June of 2000.

5.2 Linearity

At the right plot in Fig. 21 the average values of signals in the central pixel versus the sum of signals from neighbour ones are shown by circles. The declination from the line behaviour is slightly visible. Rectangles show the same dependence but for the calculated variances of signals for each LED amplitude. For signals lower then 30–50 *ph. el.* the variance follows statistical fluctuations $(\delta n)^2 = n$. For larger amplitudes the saturation of PMT gain becomes distinguishable. The PMT was operated at 850 V bias and anode load 50 Om coaxial cable. In Fig. 22 the standard deviation of LED signal in all 34 read–out channels is plotted vs peak position. For almost all channels signal starts saturation at 50 ADC counts.

The duration of LED pulse was $\sim$ 30 *nsec* for the peaking time and $\sim$ 80 *nsec* at the base line. During the tests described above the signal was integrated over 150 nsec. Taking into account that particle time response is faster than LED one, the gain saturation is to start earlier for physical data.

The possible way to cope with the problem of PMT saturation is to exploit it at lower bias. To compensate the signal drop a higher load could be used. This issue is in direct connection with the design of the front–end electronics [8]-[9] and should be optimised in the future developments.

In spite of the large X–talk values and poor linearity of PMT photo–readout, the measured performances such as the discrimination of pions, ECAL energy corrections and MIP registration efficiency of the SPD/PS prototypes are compatible with major LHCb requirements.

6 Durability and radiation hardness of PS/SPD

It is well known, that bended at small radius plastic fibres loose light due to the curvature and due to the cracks caused by mechanical stresses in the fibre cladding.

S–type fibers from KURARAY show advanced mechanical durability [7] and can be used for a small bending radius about 2 cm. It is an experimental problem, how to specify the method allowing to prove the durability over ten years of operation. We plan to provide some particular test to apply the technique of aging accelerated by heating.

The radiation hardness of scintillator/fibre systems is a well studied subject. The radiation environment of the preshower detector is $2-3$ times lower due to absorbed dose Z-profile than in ECAL, that contains essentially the same materials. Therefore, one should not expect significant degradation of PS response over 10 years of operation. In case of an extreme irradiation the very inner part of the detector could be easily replaced, as it is foreseen by the mechanical design [2]. Nevertheless, some additional tests of the radiation hardness of bended fibre glued in the polystyrene scintillator is appreciable to quantify the degradation rate.

7 Summary and plans for future tests

Acceptable level of performance have been achieved with the SPD/PS prototypes in the tests in 1999. Design of fibre layout is fixed by optimisation of the light collection. The WLS fibre is coiled in "DEEP" groove with 3 loops and glued with optical glue. This allows to achieve 20 and 30 ph. el. per MIP for large and small cells in the full scale prototype. There are few items to be completed in coming tests:

- Optimisation of the fibre-to-PMT coupling to minimise the light X-talk in PMT.
- Performance of prototypes should be studied with fast electronics close to the final read-out.
- Accelerated aging tests of fibre/scintillator.
- Degradation rate under irradiation of the coiled fibres glued in the scintillator.
- Design optimisation of fibre-to-fibre connectors.

Acknowledgements

The authors wish to thank all the members of the LHCb Calorimetry group, whose constant interest inspired our studies. We thank Jacques Lefrancois, Pascal Perret and Andreas Schopper for carefully reading the manuscript and useful comments. We are grateful to the CERN staff who provided us with the beam facilities under the best conditions. In particular we are much indebted to Rolf Lindner and Peter Schilly for the constant help in prototypes and experimental zone preparation.

References

[1] LHCb Collaboration, LHCb Technical Proposal, CERN/LHCC 98–4 (1998).

[2] S. Filippov *et al*, Design and Construction of the LHCb Scintillator Pad/Preshower Detector, LHCb 2000–42.

[3] V.I. Kryshkin, A.I. Ronzhin,*et al*, NIMA 247 (1986) 583. CDF II Detector TDR, FERMILAB-Pub-96/390-E,1996; G. Aguillion *et al*, NIMA 417 (1998) 266; M.M. Aggarwal *et al*, hep–ex/9807026, 1998

[4] HAMAMATSU Photonics KK, Electron Tube Center, 314-5, Shimokanzo, Toyooka-village, Iwata-gun, Shizuoka-ken, 438-01 Japan.

[5] BICRON Corp., 12345 Kinsman Rd. Newbury OH 440 USA

[6] KURARAY Corp., 3-10, Nihonbashi, 2 chome, Chuo-ku, Tokyo, Japan.

[7] K. Hara *et al*, NIMA 411 (1998) 31.

[8] S. Bota *et al.*, Scintillator Pad Detector Front-End Electronics, LHCb 2000-027, CALO.

[9] G. Bohner *et al*, Very Front-End Electronics for LHCb Preshower, LHCb 2000–47, CALO.

[10] S. Aota *et al*, NIM A357 (1995) 71.

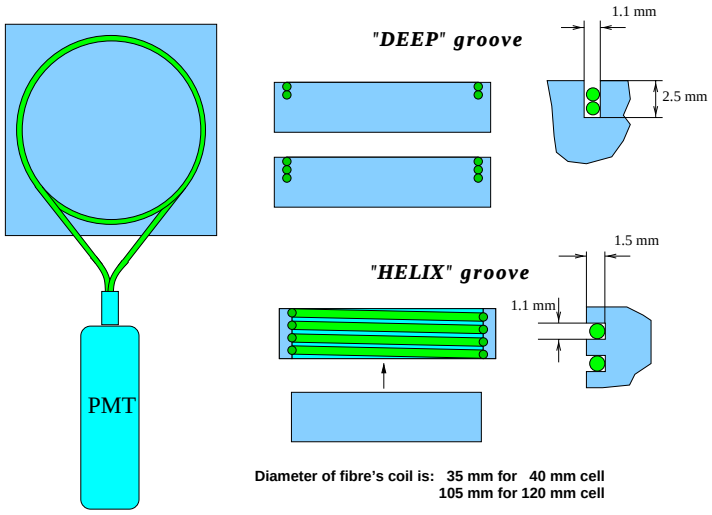

Figure 1: Design of preshower prototypes.

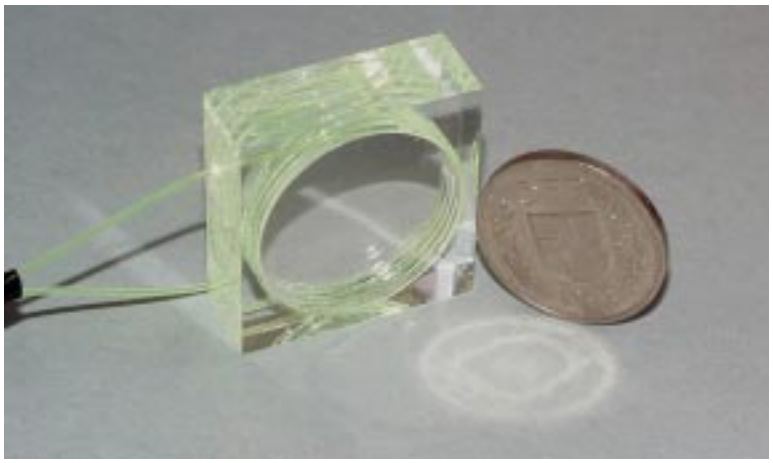

Figure 2: Preshower prototype with the "HELIX" groove. The fibre runs through scintillator by spiral.

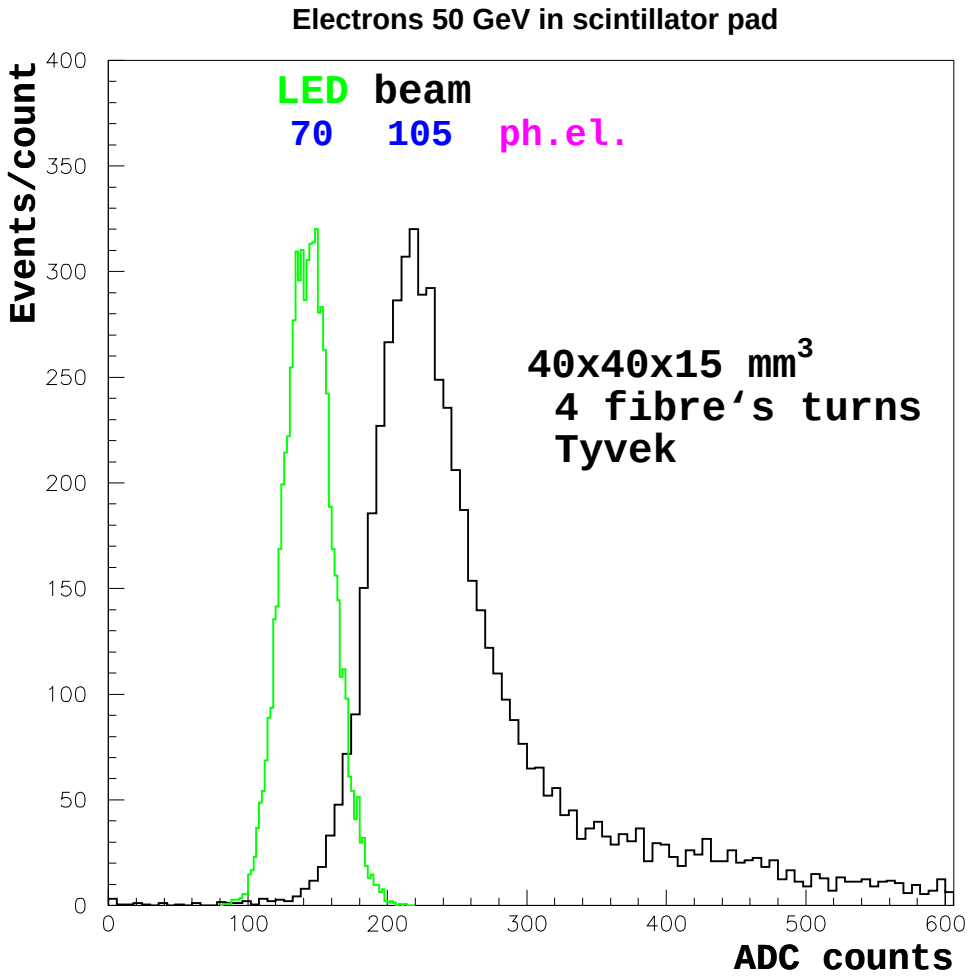

Figure 3: The signal from 50 GeV electrons in polystyrene scintillator pad fig 2 of $4cm \times 4cm \times 15mm$ size read-out by 4 coils of 1mm diameter Y11(250)MC S-type fibre glued in "vertical groove" and coupled to the PMT with 15% quantum efficiency is shown. **No clear fibre** was used. Pedestal is subtracted. Comparison with LED signal gives $\sim$ 105 photo electrons at the peak.

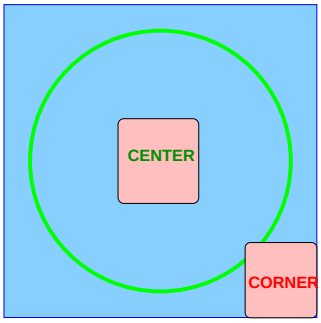

Figure 4: Uniformity study of 120 × 120 mm^2 cell. Beam position at centre and corner of cell.

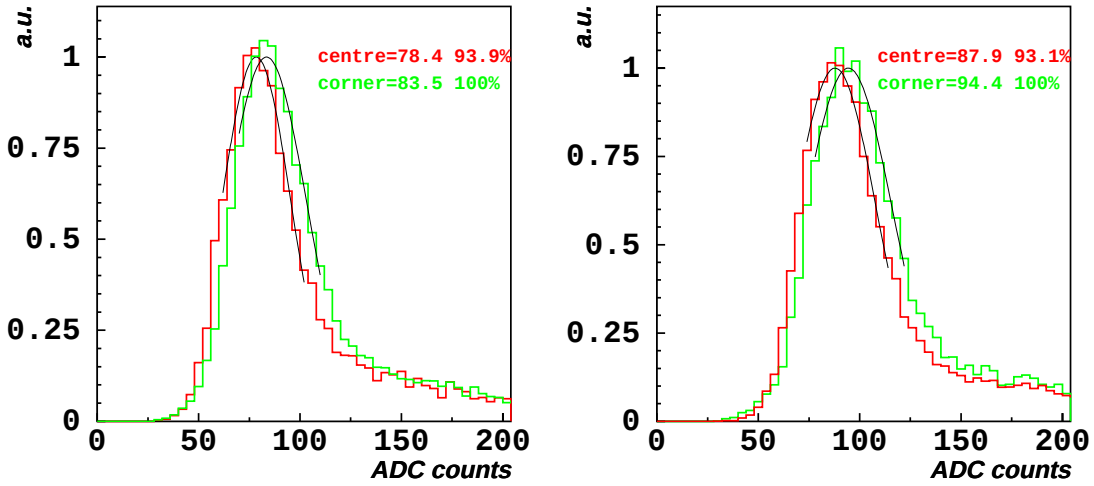

Figure 5: Uniformity study of 120 × 120 mm^2 cell. Signal is compared at the centre and at the corner of the cell. Two prototypes with "DEEP" groove: **(left)**) 2 fibre turns and **(right)**) 3 fibre turns.

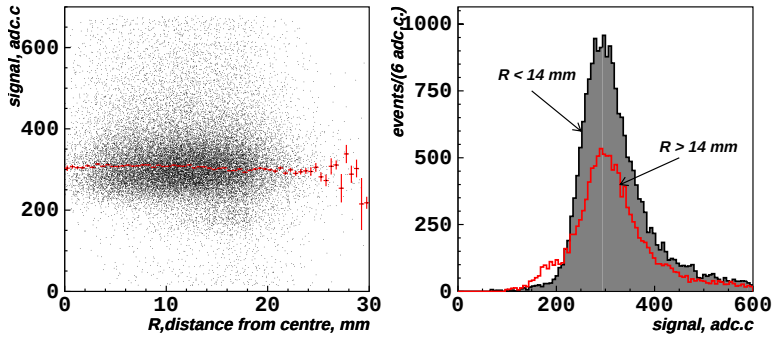

Figure 6: Uniformity of response in $10 \times 40 \times 40$ mm^3 cell with 4 fibre coils in "DEEP" groove.

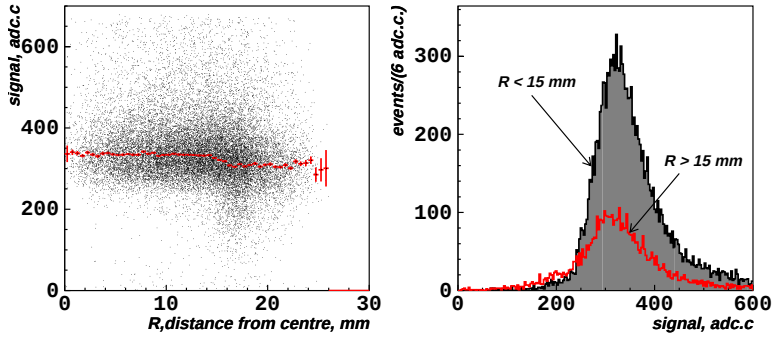

Figure 7: Uniformity of response in $15 \times 40 \times 40$ mm^3 cell with 4 fibre coils in "HELIX" groove.

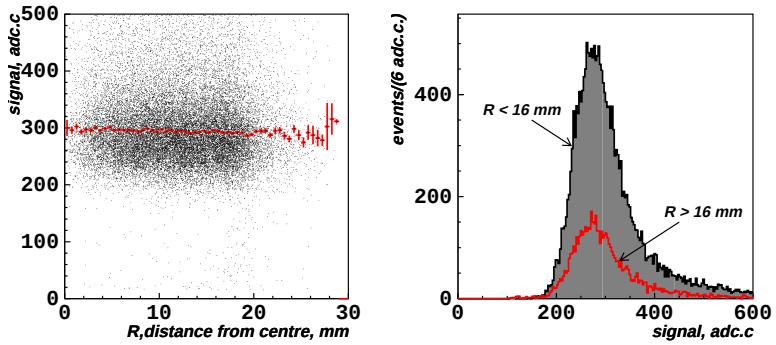

Figure 8: Uniformity of response in $15 \times 40 \times 40$ mm^3 cell with 2 fibre coils in "DEEP" groove.

Figure 9: Common view of assembled prototypes. Ends of WLS fibres are equipped with optical connectors. Bundle of clear cables is inserted in light isolating tube. 3m clear fibres go to special optical connector which provides precise positioning fibres to corresponding PMT anode pixels.

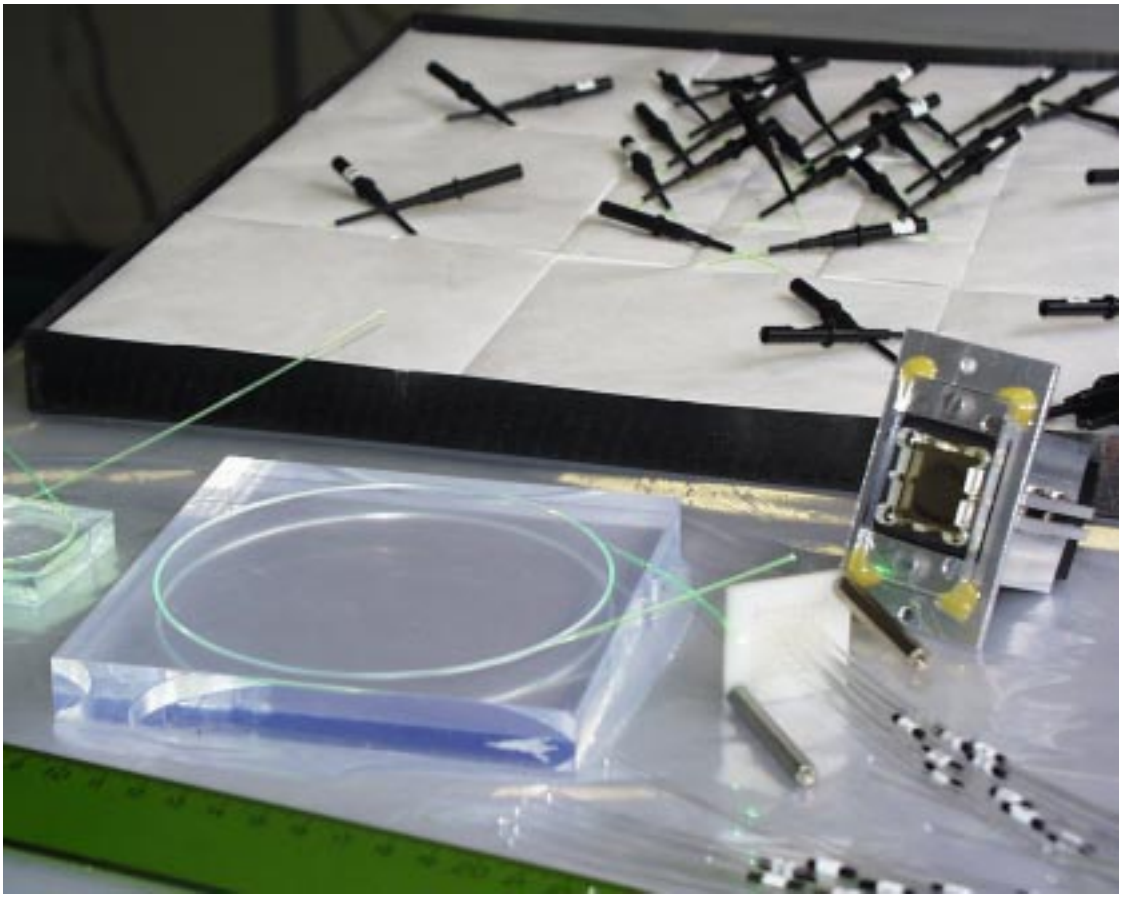

Figure 10: View of 12 and 4 cm cells with glued fibre in "DEEP" groove is shown. WLS Y11(250) S-type fibre makes 3 loops inside scintillator. Scintillator was wrapped by 150 μm TYVEK paper. One can see also PMT housing with plastic frame glued to housing box from window side. The position of the frame was aligned to provide correct fibre-to-PMT connection.

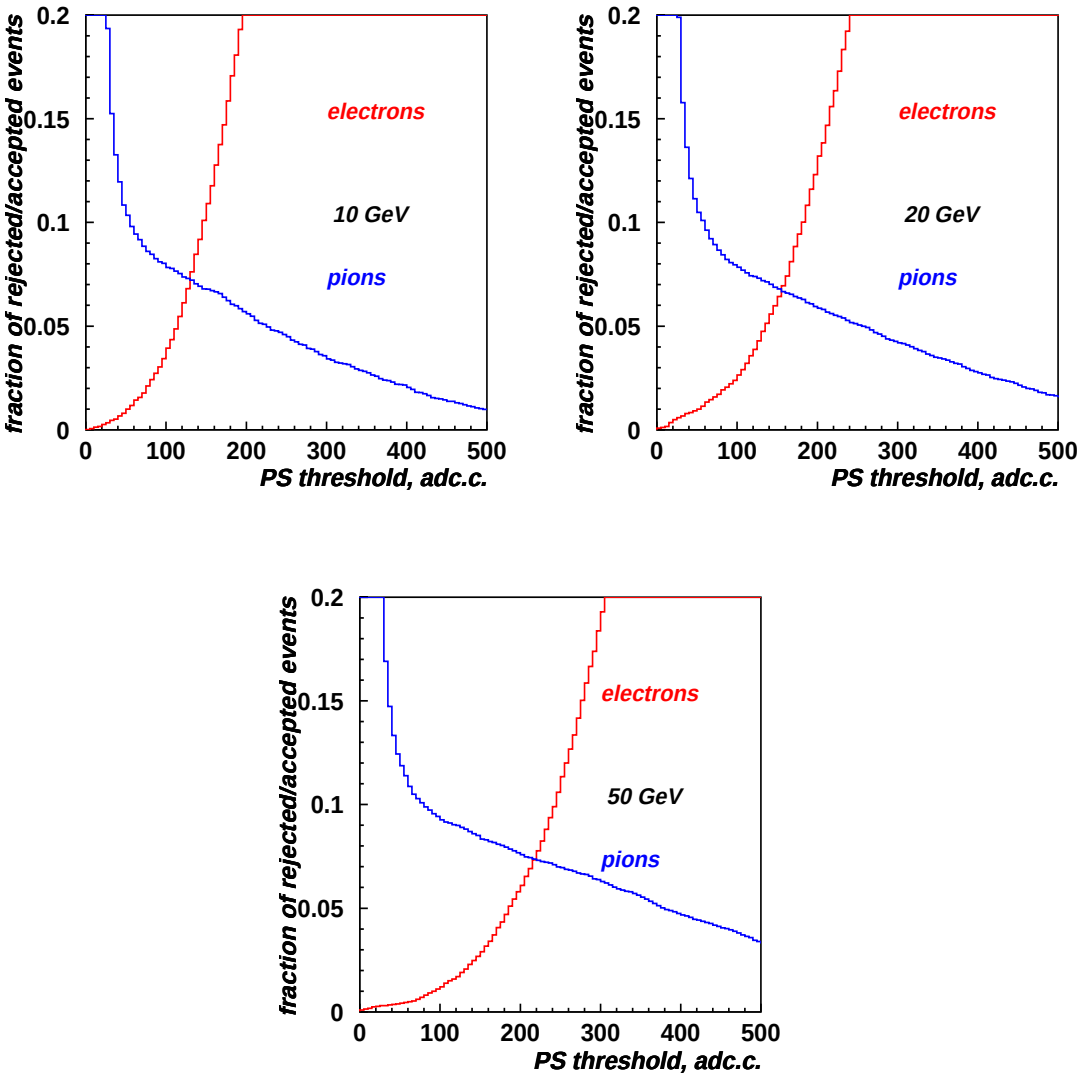

Figure 11: π/e rejection with PS.

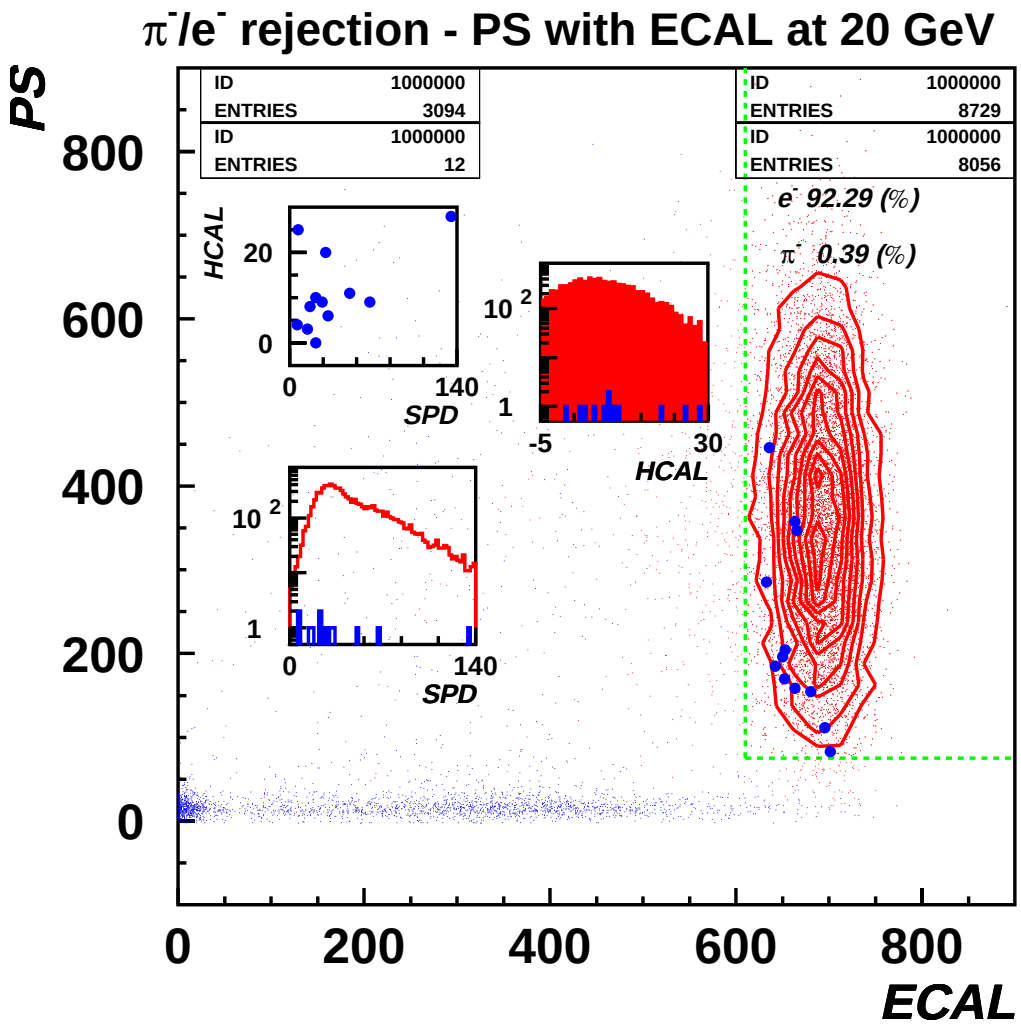

Figure 12: π/e rejection with PS and ECAL.

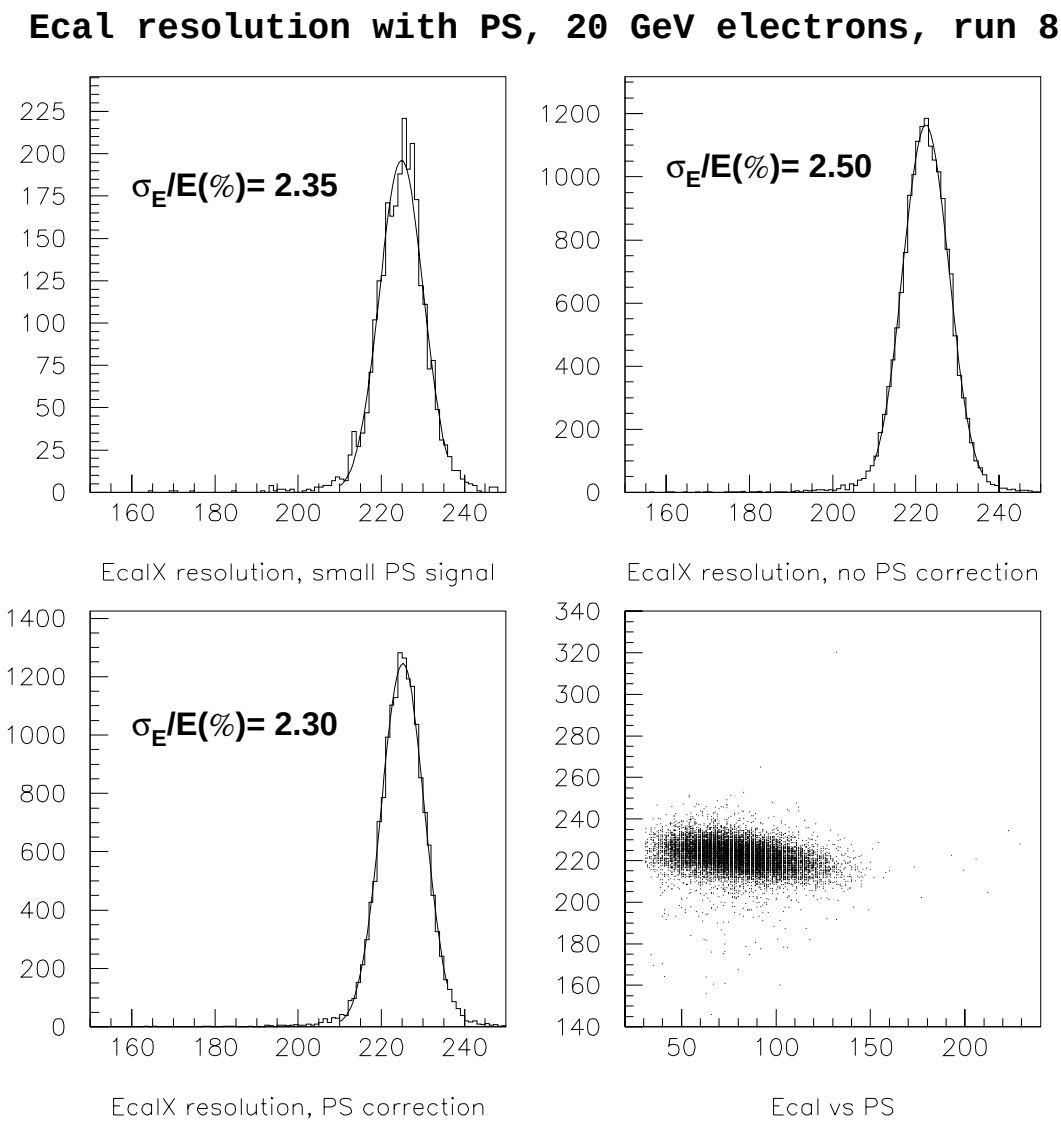

Figure 13: Energy resolution of ECAL with PS. Electrons, 20 GeV/c.

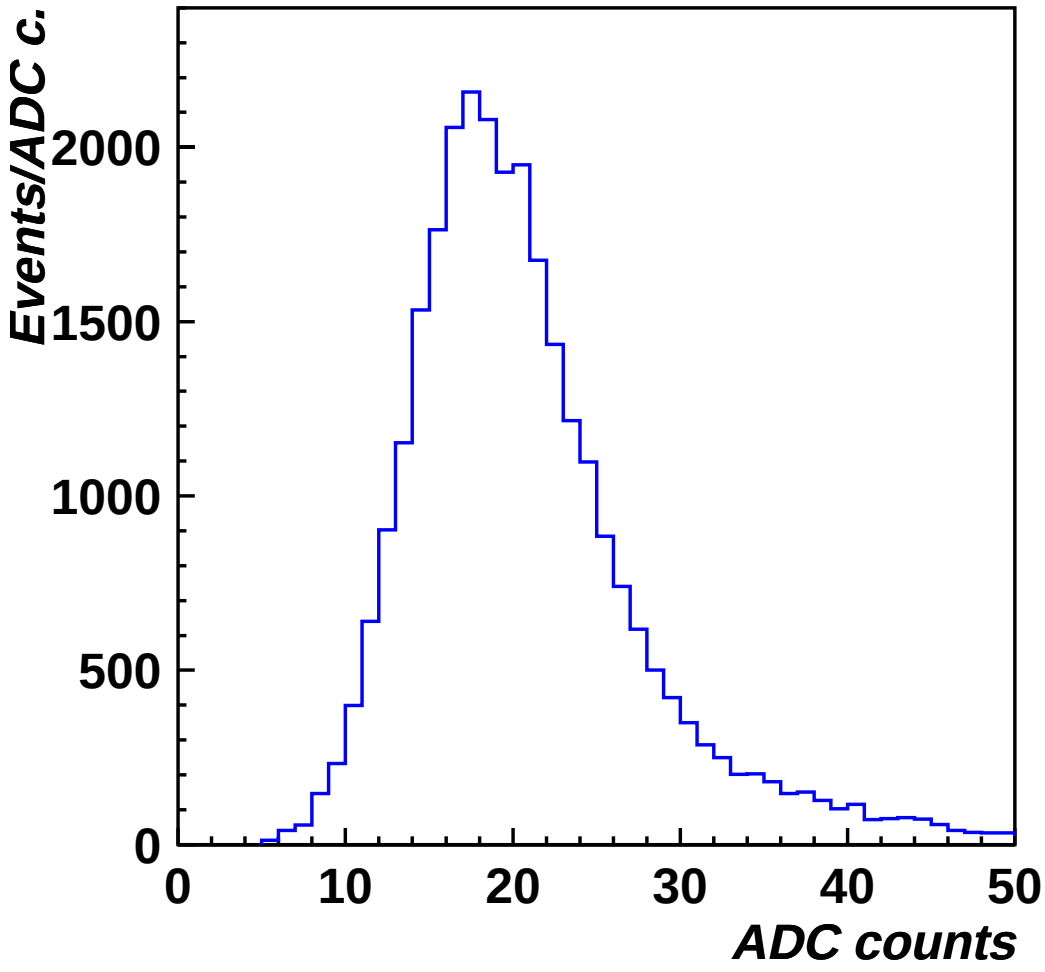

Figure 14: Pions of 20 GeV energy in SPD.

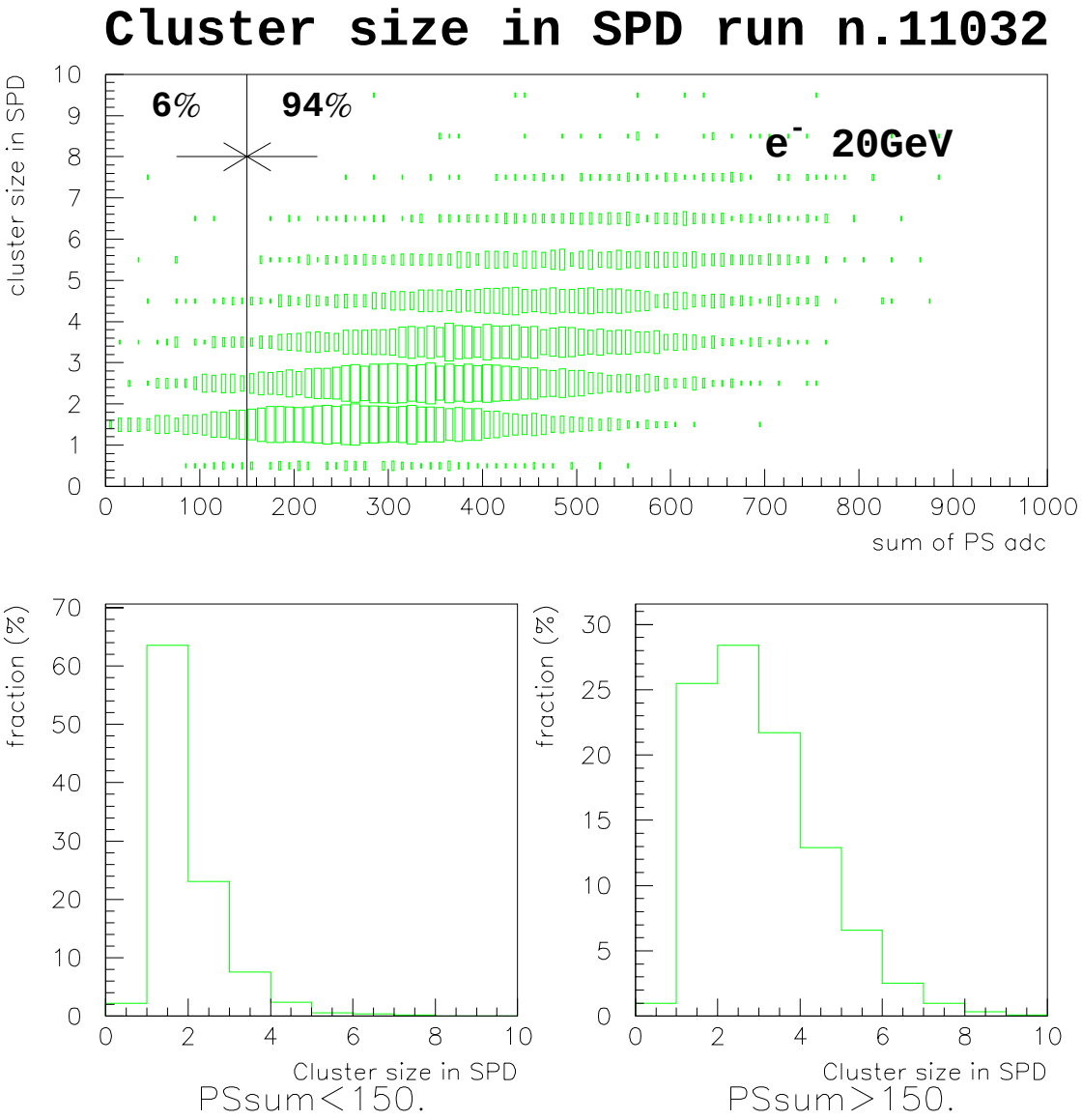

Figure 15: Electrons, 20 GeV/c.

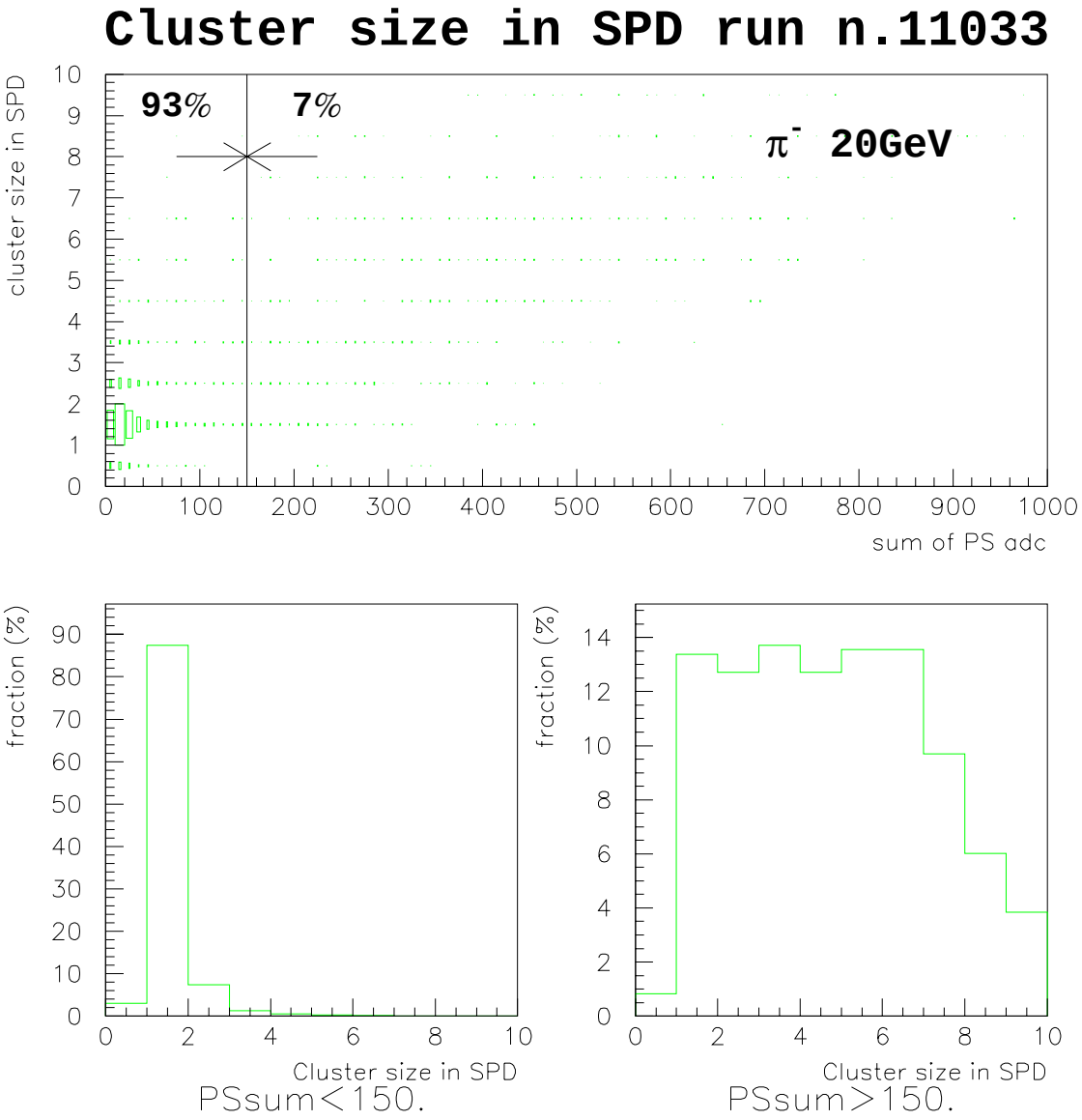

Figure 16: Pions, 20 GeV/c.

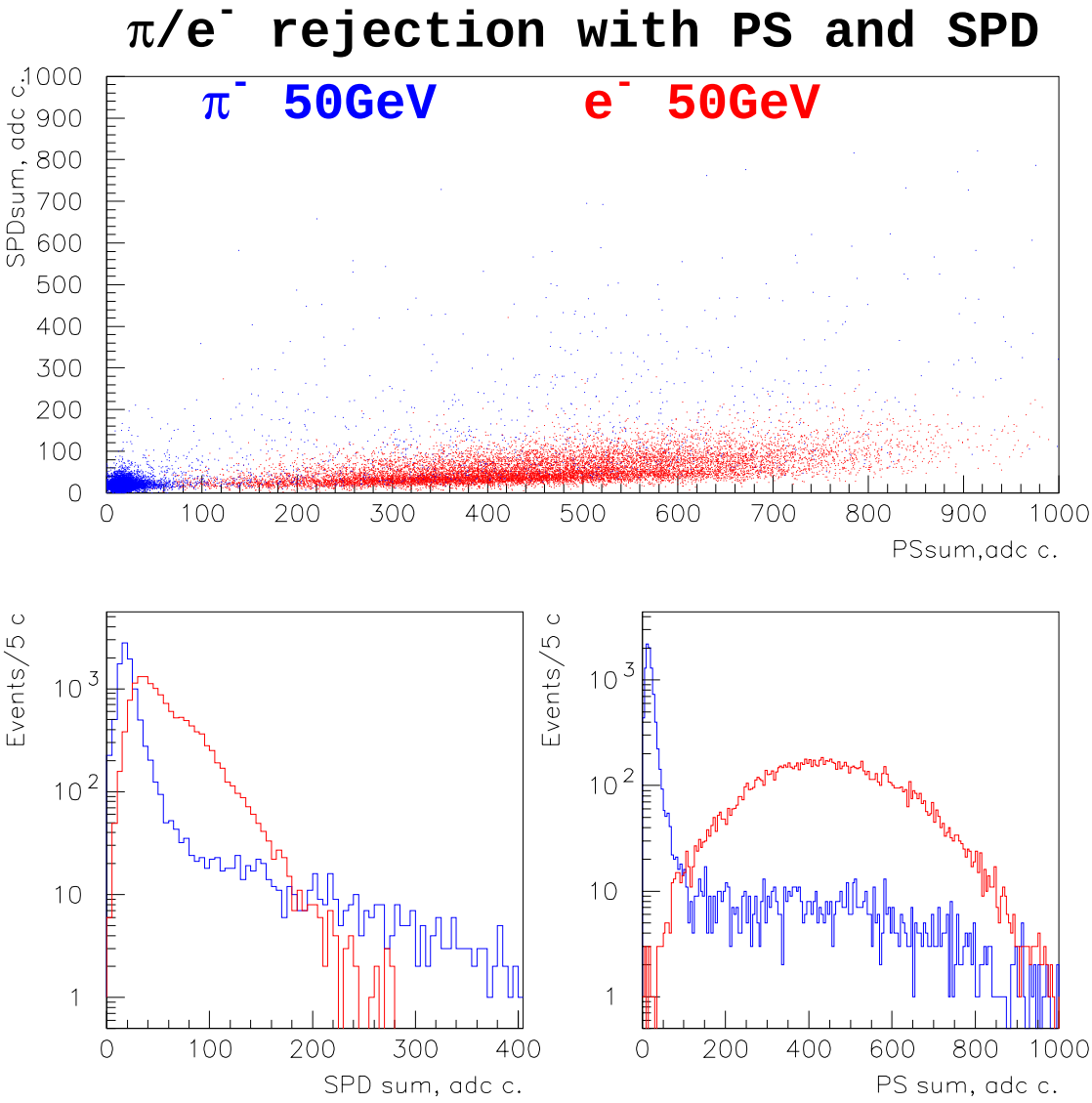

Figure 17: Pion rejection with SPD and PS.

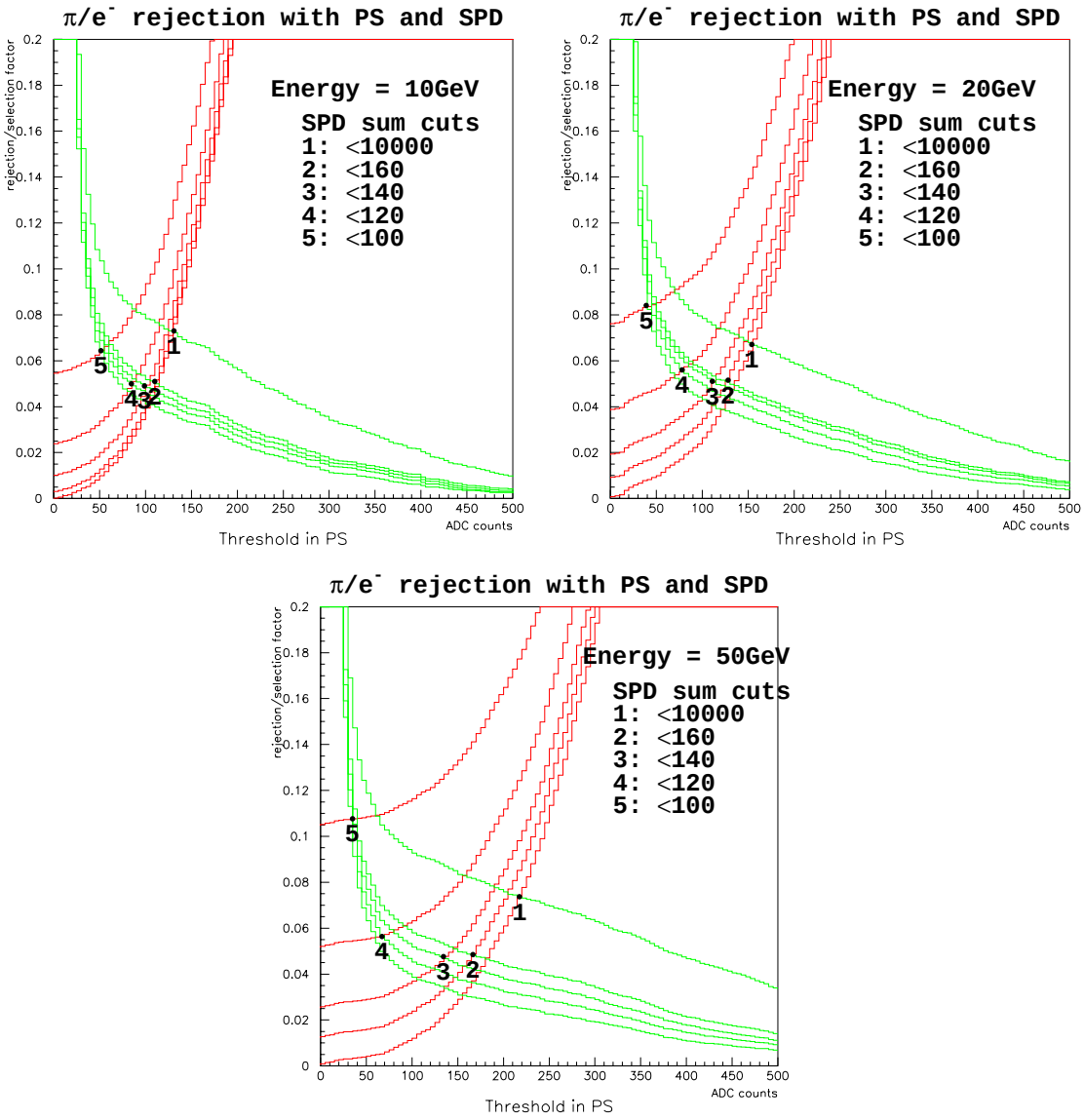

Figure 18: π/e rejection with PS and SPD.

HV INPUT •

77	85	83	90	96	90	100	92
63	78	82	75	76	81	92	79
63	78	74	66	70	75	89	75
64	76	75	69	68	72	84	76
66	79	76	67	67	53	79	73
73	82	82	73	71	74	81	72
66	87	85	80	69	81	86	76
76	80	78	87	94	92	90	79

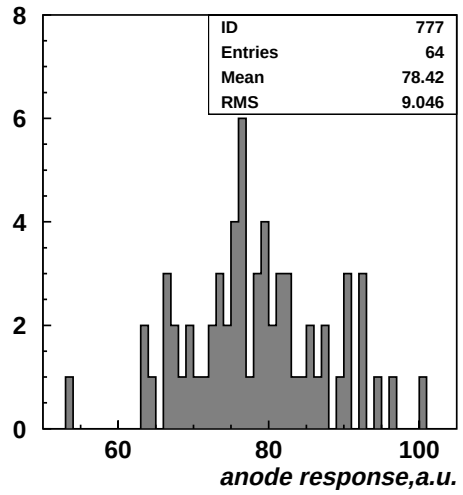

Figure 19: Uniformity of H7546 MaPMT anode response measured by manufacturer. Ratio of max/min values ~ 2, variation 12%(rms).

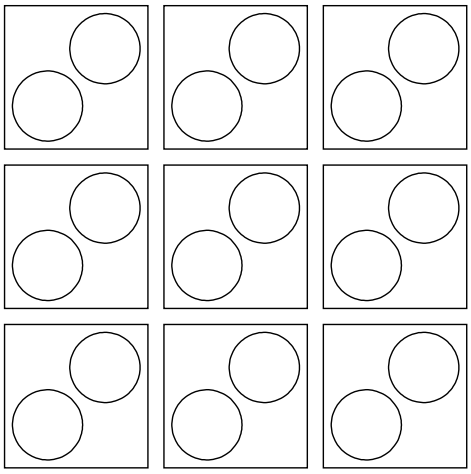

Figure 20: Fibre-to-pixel connection. Layout of holes with respect to PMT pixels. The distance from the fibre edge to the pixel boundary is 0.1 mm.

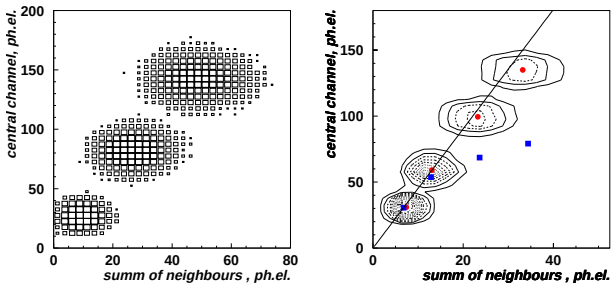

Figure 21: **Left:** LED illuminates the fibre coming to the pixel N12. Signal from pixel N12 is plotted vs the sum of signals from neighbour 8 pixels for 3 various LED amplitudes. About 25% of light from the illuminated fibre comes to the adjacent pixels. Photo-statistical fluctuations of leakage has no visible correlation with central pixel signal. **Right:** The same as on the left, but for pixel N13. Light leakage is about 20%. Circles mark the mean value of signals for each LED amplitude. Rectangles show the same dependence but for the calculated variances of signals for each LED amplitude. For amplitudes lower then 30-50 ph. el. it follows the statistical fluctuations $(\delta n)^2 = n$. For larger amplitudes the saturation of the PMT gain becomes distinguishable. The PMT bias was 850 V.

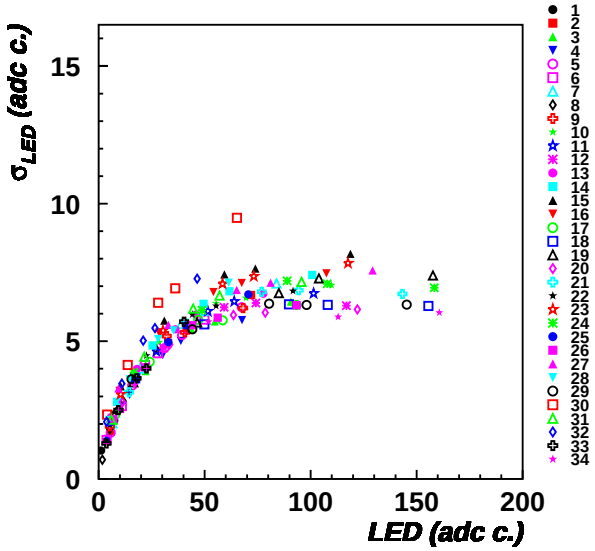

Figure 22: LED was flashing on all the fibres coming to 34 read-out PMT pixels. Standard deviation of the each pixel signal is superimposed vs peak position. For almost all channels PMT gain saturates above ~ 50 adc counts ($\sim 50 - 60$ ph.el.).